JOURNAL OF MATERIALS SCIENCE 20 (1985) 2603–2613

Microstructure and mechanical properties of metastable lath martensite wires in the Fe–Ni–Cr–Al–C system produced by melt spinning in rotating water

A. INOUE, H. TOMIOKA*, T. MASUMOTO
The Research Institute for Iron, Steel and Other Metals, Tohoku University, Sendai 980, Japan

Metastable lath martensite (α'_L) phase wires with high strengths have been produced in the Fe–Ni–Cr–Al–C alloy system by melt spinning in rotating water. These wires have a circular cross section and a white lustre and the wire diameter is in the range of 100 to 140 μm. The width and length of each lath in the α'_L phase are as small as about 0.3 and 2 μm, respectively. The σ_y, σ_f and ϵ_p are about 900 and 1650 MPa and 2.0% for the α'_L wires. The subsequent annealing causes an increase in ϵ_p as well as σ_y and σ_f and the attained values are about 1000 and 1700 MPa and 3.0% for Fe–10 Ni–10 Cr–6.5 Al–1.0 C wire annealed at 773 K for 1 h owing to the precipitation strengthening of a very fine unidentified carbide and to a high density of dislocations and lath boundaries in the α'_L phase. Further annealing causes a significant decrease in ϵ_p through decomposition of α'_L to $\alpha + M_7C_3 + M_{23}C_6$. Therefore, the high strength combined with relatively good ductility for the α'_L wires is interpreted as due to the suppression of the phase transformation of α'_L to a mixed structure of $\alpha + M_7C_3 + M_{23}C_6$ by melt quenching.

1. Introduction

Recently, with an aim to produce fine-gauge ferrous wires exhibiting high static and dynamic strengths and good ductility combined with high corrosion resistance directly from the liquid state without intermediate processes, the present authors carried out extensive and systematic investigations [1–8]. The preparation conditions for producing a continuous wire directly from the melt by a technique using melt spinning into rotating water, the development of alloy compositions which are appropriate for the melt-spinning method, and the mechanical strengths, ductility, corrosion resistance and thermal stability of the wires thus produced were studied. As a result, they have succeeded in obtaining ultra-high strength ferrous wires having a good ductile nature and high corrosion resistance [6–8] and there is a high possibility that the wires might be used practically as fine-gauge high strength materials owing to the many advantages of the low cost of the production of the wires as well as the characteristics of the wires described above. The melt-quenched structure of these wires is composed of γ single phase or the duplex γ phase contaning a small amount of carbide, intermetallic compound or lath martensite.

It is well known that low carbon maraging steels with high strength and good toughness possess a tempered lath martensite structure dispersed with intermetallic compounds with very fine particle size. The formation of lath martensite

*Permanent address: Research and Development Centre, Unitika Ltd, Uji 611, Japan.

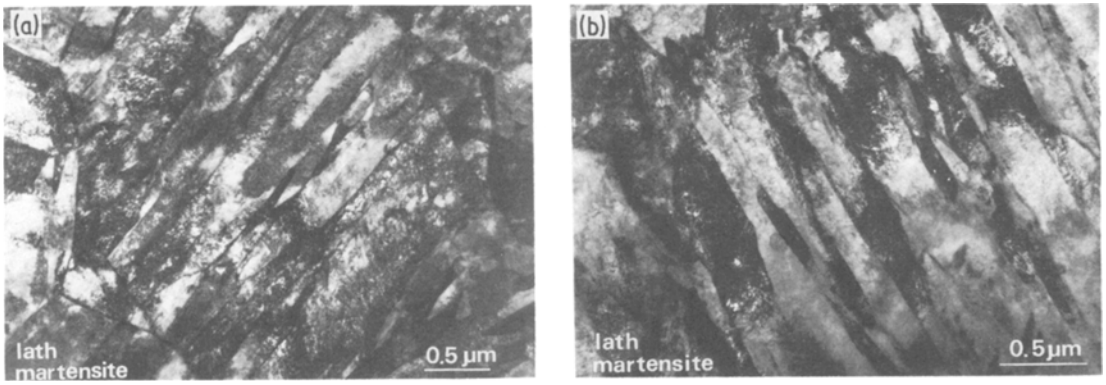

Figure 1 Transmission electron micrographs showing the lath martensite structure of melt-quenched Fe–10Ni–10Cr–6.5Al–0.8C (a) and Fe–10Ni–10Cr–6.5Al–1.0C (b) alloys.

wire containing a large amount of solute elements by rapid quenching from the liquid is expected to result in the appearance of the maraging-type wires having high strength and good ductility by tempering the lath martensite structure. However, the application of the in-rotating-water spinning technique to conventional maraging steels did not result in the formation of a continuous wire having a good white lustre [9], indicating the necessity that one must find alloy compositions which are appropriate for the direct formation of the wire from the liquid state. The purpose of this paper is to examine the melt-quenched structure of Fe–Ni–Cr–Al–C and Fe–Ni–Cr–Al–C–X (X = Nb, Ta, Ti or Zr) alloys and the change in the melt-quenched structure on annealing and to investigate the possibility of whether or not the simple process of melt-quenching followed by the subsequent annealing leads to a similar structure and strengths as those of conventional maraging steels, which have been fabricated through many complicated processes.

2. Experimental methods

Fe–Ni–Cr–Al–C and Fe–Ni–Cr–Al–C–X (X = Nb, Ta, Ti, or Zr) alloy ingots with different compositions were prepared under an argon atmosphere in an induction furnace from pure metals and white cast iron. The alloy composition ranges from 7 to 12.5 at% Ni, 8 to 12.5 at % Cr, 5 to 7.5 at% Al, 0.8 to 1.6 at% C and 0 to 4 at% X. The weight of the mixture melted in one run was about 40 g and the melt was transfered into a quartz tube of about 6 mm inner diameter and solidified in the tube. The compositions of alloys reported are the nominal ones denoted by atomic percentage, since the difference between nominal and chemically analysed compositions is less than 0.04 wt% for chromium, aluminium, carbon, niobium or tantalium. From a small piece of the master ingot, a long ribbon with a cross section of about 3 mm × 100 μm was prepared by single roller type melt-spinning apparatus as the test sample for the structural observation. The amount of alloy melted in a run was about 5 g, and the rotation speed of the steel roller (20 cm diameter) was controlled at about 800 r.p.m. In addition, a continuous wire, diameter 100 to 140 μm, was prepared as the sample for measuring mechanical properties, by using the in-rotating-water melt spinning technique [10, 11] which is capable of producing a wire with a circular cross section directly from the molten metal. The details of the operating parameters in this technique are the same as those [6, 7] for the production of the austenite wires in the Fe–Ni–Cr–Al–C system. Furthermore, the methods of characterizing the crystal structure, microstructure and fracture surface morphology by X-ray, optical and electron metallographic techniques and of measuring yield strength (σ_y), tensile fracture strength (σ_f), and elongation (ϵ_p) of the wire samples have been described elsewhere [2].

3. Results and discussion

3.1. Formation range and microstructure of lath martensite (α'_L)

Fig. 1 shows the as-quenched structure of (a) Fe–10 Ni–10 Cr–6.5 Al–0.8 C and (b) Fe–10 Ni–10 Cr–6.5 Al–1.0 C alloys. The structure is composed of lath martensite containing an extremely high density of dislocations and the average width and length of each lath are as small as ~ 0.3 and 2 μm, respectively. No distinct splitting

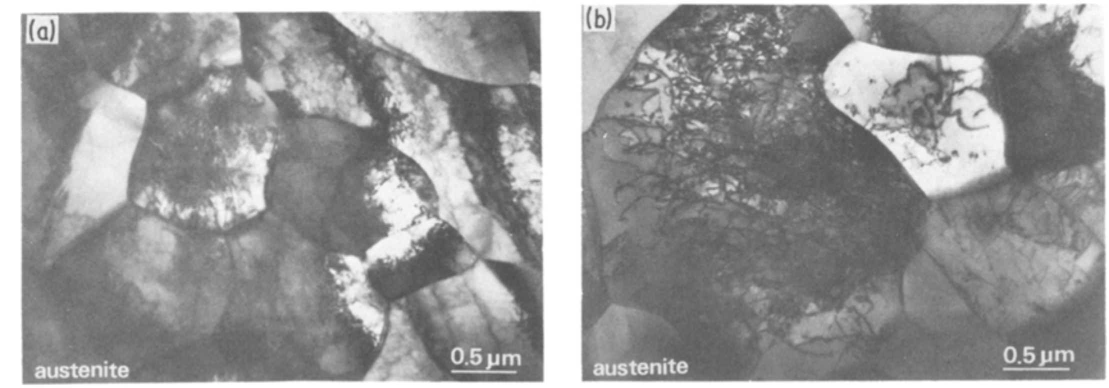

Figure 2 Transmission electron micrographs showing the austenite structure of melt-quenched Fe–12.5Ni–10Cr–6.5Al–1C (a) and Fe–10Ni–10Cr–6.5Al–1.6C (b) alloys.

of the reflection spots of 110, 200, 211 on the electron diffraction patterns taken from the lath martensite is observed and hence the crystal structure of the lath martensite appears to be a bcc structure with a lattice parameter of about 0.288 nm or a bct structure with a ratio of $c/a \simeq 1$. Furthermore, no trace of austenite phase is observed even in the electron diffraction patterns, indicating that the M_f as well as M_s point of these alloys is above room temperature. The increase in nickel and/or carbon content above about 12.5 at% Ni or 1.6 at% C results in a complete disappearance of lath martensite phase and the formation of an austenite single phase with an average grain size of 1 to 2 μm as shown in Fig. 2a and b. Judging from the fact that the usually solidified structure of Fe–10 Ni–10 Cr–6.5 Al–(0.8–1.0) C alloys exhibits a mixed structure of ferrite and $M_{23}C_6$ carbide, the lath martensite is concluded to be in a nonequilibrium state. These results demonstrate that the cooling rate ($\simeq 10^4 - 10^5$ K sec^{-1}) achieved by the present melt quenching could be sufficiently high to suppress the phase transformation of α'_L-Fe to α-Fe and also the precipitation of $M_{23}C_6$ carbide.

The composition range in which the lath martensite forms in Fe–Ni–10 Cr–6.5 Al–C system is outlined in Fig. 3, where the formation ranges of other quenched phases are also represented for reference. The formation of the lath martensite is limited to the range of 0.7 to 1.5 at% C and 7 to 11 at% Ni. The size of the lath martensite tends to decrease slightly with increasing carbon and nickel content probably because of the lowering of the M_s and M_f points. Fig. 3 also shows that the further increase in nickel and/or carbon content results in the structural change of α'_L to $\alpha'_L + \gamma$ and then to γ, while a further reduction of nickel and/or carbon content leads to an increase in difficulty of the ejection of the molten metal through orifice of the nozzle and to the disappearance of the white lustre of the ejected ribbons. Here it appears important to point out that all the melt-quenched α'_L ribbons with a thickness of about 100 μm exhibit a good ductility, which is defined by a 180° bending.

Additionally, the effect of additional elements (Nb, Ta, Ti, or Zr) on the microstructure of the lath martensite in Fe–10 Ni–10 Cr–6.5 Al–1 C alloy was examined with an aim to achieve a further refinement of lath martensite. As examples, Fig. 4 shows the change in as-quenched structure of Fe–10 Ni–10 Cr–6.5 Al–1 C–Nb alloys with increasing niobium content. For the 1 at% Nb

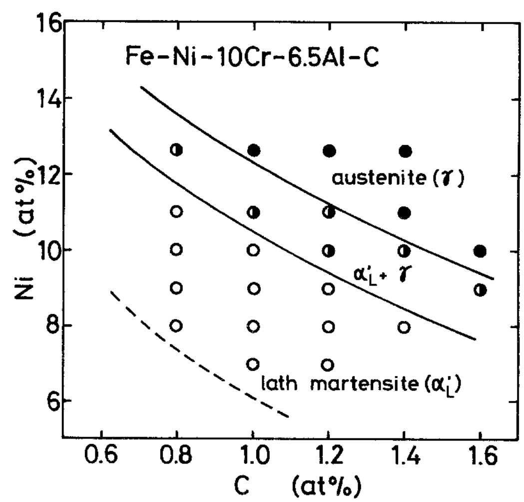

Figure 3 Compositional dependence of melt-quenched structure of Fe–Ni–10 Cr–6.5 Al–C alloys.

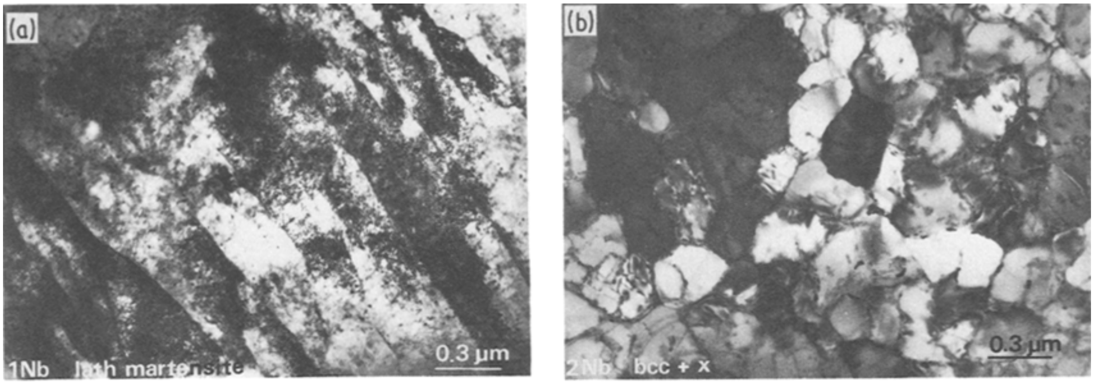

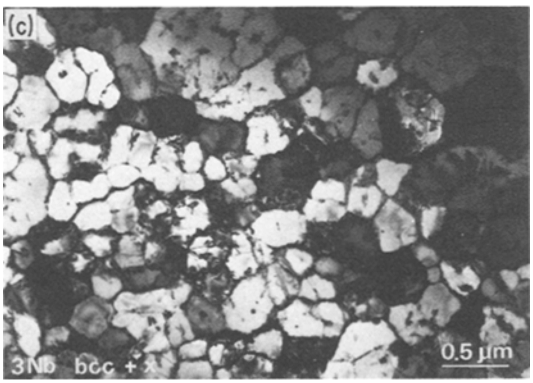

Figure 4 Transmission electron micrographs showing the melt-quenched structures of Fe–10 Ni–10 Cr–6.5 Al–1 C–1 Nb (a), Fe–10 Ni–10 Cr–6.5 Al–1 C–2 Nb (b) and Fe–10 Ni–10 Cr–6.5 Al–1 C–3 Nb (c) alloys.

alloy, the lath martensite is formed and the internal structure and the lath size remain almost unchanged, even though the black contrast suggesting the existence of very fine precipitates becomes clearer. The further addition of niobium results in a drastic change in as-quenched structure from α'_L to ferrite (α) having a size as small as about 0.2 μm as seen in Fig. 2b and c. This indicates that the addition of niobium reduces very significantly the formation range of austenite in the high temperature range probably because niobium itself is a strong ferrite-forming element and the strong interaction between niobium and carbon reduces the effective carbon content in the alloys. A similar change in the as-quenched structure was also observed in the cases of the addition of tantalum, titanium, or zirconium and the critical additional amount, which causes the change from α'_L to α, was judged to be 2 at% for tantalum and 1 at% for titanium or zirconium.

3.2. Annealed microstructure

Since the lath martensite in Fe–Ni–Cr–Al–C system produced by the melt-quenching technique is a nonequilibrium solid solution saturated with the substitutional elements of nickel, chromium and aluminium and the interstitial element of carbon, the subsequent annealing is expected to cause a homogeneous precipitation of fine intermetallic compound and/or carbide on the high density of dislocations, leading to a significant enhancement of mechanical strengths.

Fig. 5 shows the change in the as-quenched structure of Fe–10 Ni–10 Cr–6.5 Al–1 C alloy on annealing for 1 h in the temperature range 673 to 973 K. As seen in Fig. 5a and b, the morphology of the lath martensite remains unchanged on annealing at 673 and 823 K, but a large number of fine black contrasts revealing the existence of precipitates are seen over the whole area. The precipitates are too small to identify their crystal structure by the selected-area electron diffraction method. A further rise in annealing temperature results in a distinct change in the morphology of lath martensite accompanied with the precipitation of the second phase; the reduction in dislocation density and the disappearance of lath boundaries as shown in Fig. 5c. The precipitates from the lath martensite in Fe–10 Ni–10 Cr–6.5 Al–1.0 C alloy annealed for 1 h at 973 K are identified as M_7C_3 and $M_{23}C_6$, as exemplified in Figs. 6b and c, and further annealing results in a complete replacement of M_7C_3 to $M_{23}C_6$ accompanied with the coarsening of $M_{23}C_6$ particles, in addition to the grain growth of ferrite and the significant decrease in dislocation density as shown in Figs. 6d and e. The average particle size of the $M_{23}C_6$ carbide is about 20 nm for 1 h, 40 nm for 12 h and 70 nm for 24 h at 973 K. Here it appears important to note from the structural point of view that the anneal-induced $M_{23}C_6$ carbide is nearly globular, and its diameter is as small

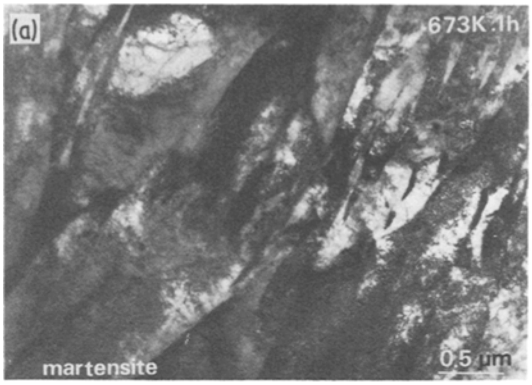

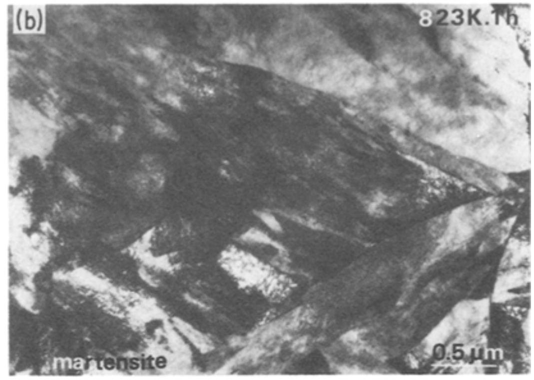

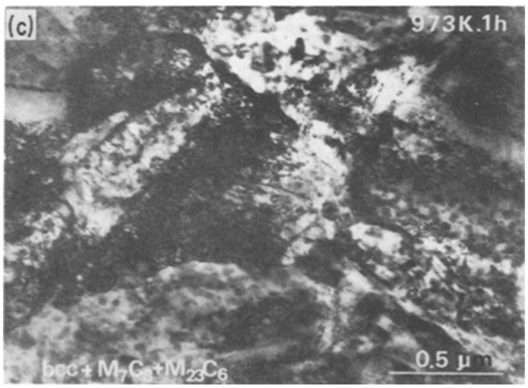

Figure 5 Change in microstructure of melt-quenched Fe–10 Ni–10 Cr–6.5 Al–1 C alloy on annealing for 1 h at (a) 673 K, (b) 823 K and (c) 973 K.

as ~20 to 70 nm and the distribution is very homogeneous throughout the α phase.

3.3. Change in mechanical properties on annealing

First the as-quenched structure and morphology of the wires produced under the conditions described by Inoue *et al.* [7] are presented. Fig. 7, for example, shows an optical micrograph showing the cross sectional structure of an Fe–10 Ni–10 Cr–6.5 Al–1 C wire. It can be seen that the wire has an almost completely circular cross section whose diameter is about 100 μm. Additionally, the as-quenched structure is composed of very fine grains, and the development of secondary dendrite arms, which are usually seen in the case of the usual casting, is suppressed owing to the high solidification speed. TEM observation of the as-quenched wire was not carried out in the present work owing to the difficulty of foil preparation. However, considering the results that there is no difference between wire diameter and ribbon thickness and that the X-ray diffraction profile of the wire having a diameter of $\simeq$ 100 μm is very similar to that of the ribbon having a thickness of about 100 μm, it is reasonably inferred that the as-quenched structure of the wire also consists of α'_L phase containing high densities of lath boundaries and dislocations.

The changes in σ_y, σ_f and ϵ_p of Fe–10 Ni–10 Cr–6.5 Al–1 C wire having the α'_L phase on annealing are shown in Fig. 8 as a function of annealing temperature. In the figure the annealed structure is also presented for reference and the values of σ_y, σ_f and ϵ_p are the average of seven measurements. σ_y increases from 650 to 1000 MPa in the vicinity of 673 K by precipitation of the fine unidentified particles, and further to 1325 MPa at about 873 K by the distinct decomposition of α'_L to $\alpha + M_7C_3 + M_{23}C_6$, followed by a significant decrease to 965 MPa at 973 K. The change in σ_f is different from that of σ_y; σ_f exhibits a maximum value of 1825 MPa at about 773 K in the duplex structure of α'_L + very fine unidentified precipitates, and decreases gradually with further increasing annealing temperature. ϵ_p increases slightly on annealing at temperatures below 773 K, exhibits a maximum value of about 3% and then decreases to about 1 at% at 873 K by the phase decomposition of α'_L to $\alpha + M_7C_3 + M_{23}C_6$ followed by an increase to about 2% by the particle growth of M_7C_3 and $M_{23}C_6$ carbides. As is evident from Fig. 8, the discrepancy of the annealing temperature at which σ_y and σ_f exhibit a maximum value is interpreted as due to the significant difference in ϵ_p at 773 and 873 K. Thus, the complete phase decomposition of α'_L to $\alpha + M_7C_3 + M_{23}C_6$ causes the significant loss in ductility, while the homogeneous precipitation of the unidentified precipitates having a size as small

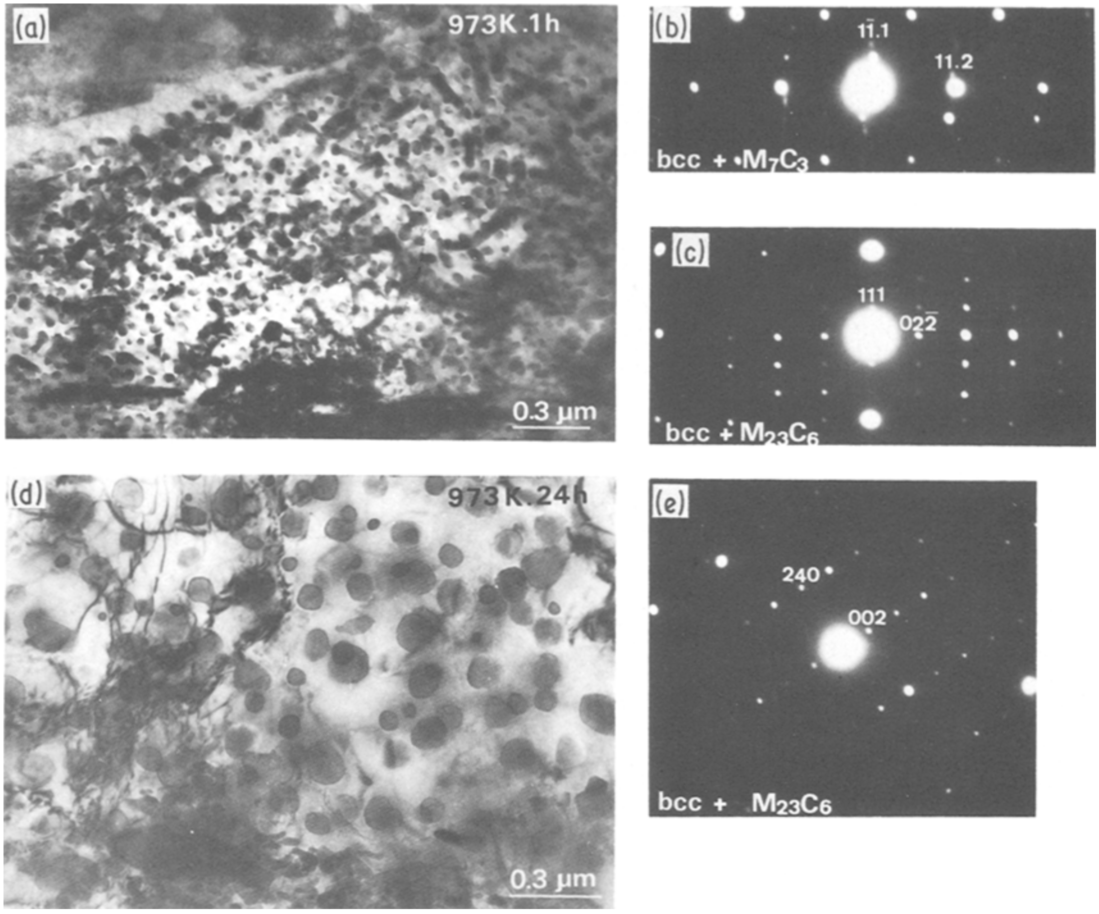

Figure 6 Bright-field images and selected-area diffraction patterns of Fe–10 Ni–10 Cr–6.5 Al–1 C alloy annealed at 973 K for 1 h (a) to (c) and for 24 h (d) and (e) after melt-quenching.

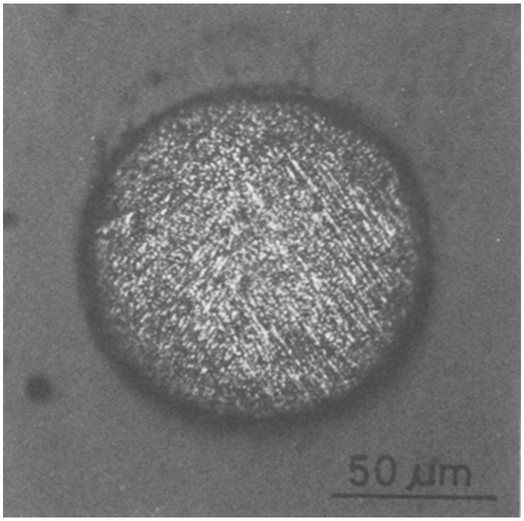

Figure 7 Optical micrograph showing the cross sectional area of Fe–10 Ni–10 Cr–6.5 Al–1.0 C wire produced by in-rotating-water spinning method.

as about 10 nm into α'_L matrix phase is very effective for the enhancement in ϵ_p as well as σ_f and σ_y. It is thus striking that the application of the appropriate annealing to the melt-quenched α'_L wires enhances both the characteristics of mechanical strengths and ductility. Accordingly, the subsequent investigation to find an appropriate alloy composition with high strength and good ductility was focused on the samples annealed at 773 K for 1 h.

3.4. Compositional dependence of mechanical properties

The σ_y, σ_f, and ϵ_p of the α'_L wires of the Fe–Ni–Cr–Al–C system in as-quenched and annealed (773 K, 1 h) states are plotted as a function of nickel, chromium, aluminium or carbon content in Figs. 9 to 12, where the amount of retained austenite (γ_R) determined by the X-ray diffraction

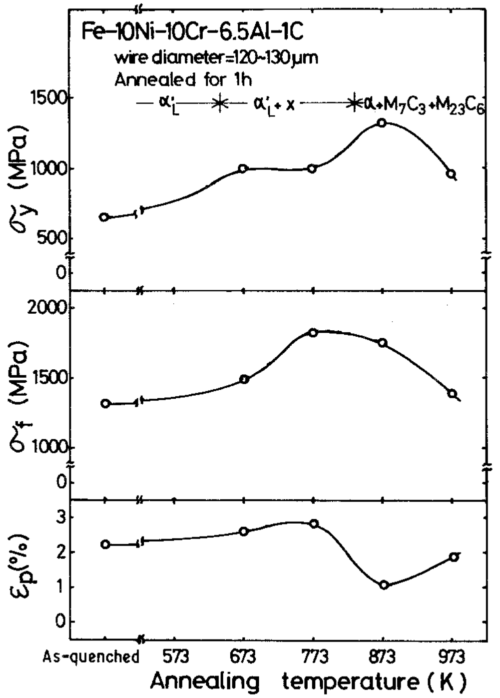

Figure 8 Changes in σ_y, σ_f, and ϵ_p of melt-quenched Fe–10 Ni–10 Cr–6.5 Al–1.0 C wire with annealing temperature.

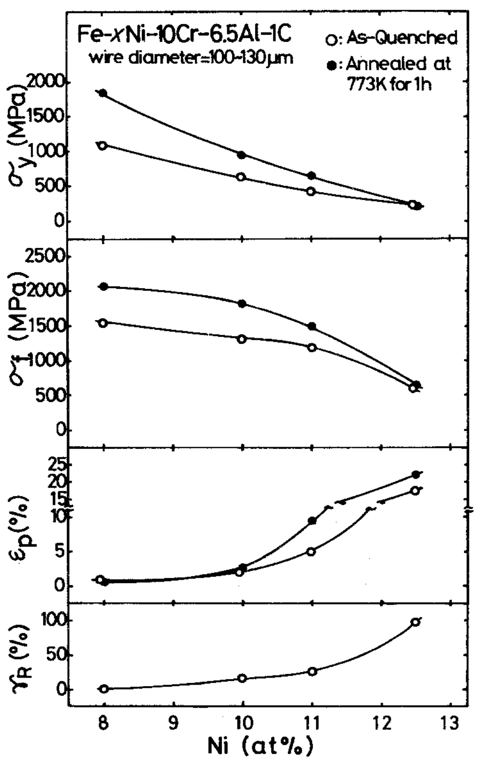

Figure 9 Changes in σ_y, σ_f, ϵ_p, and γ_R of melt-quenched Fe–Ni–10 Cr–6.5 Al–1.0 C wires with nickel content.

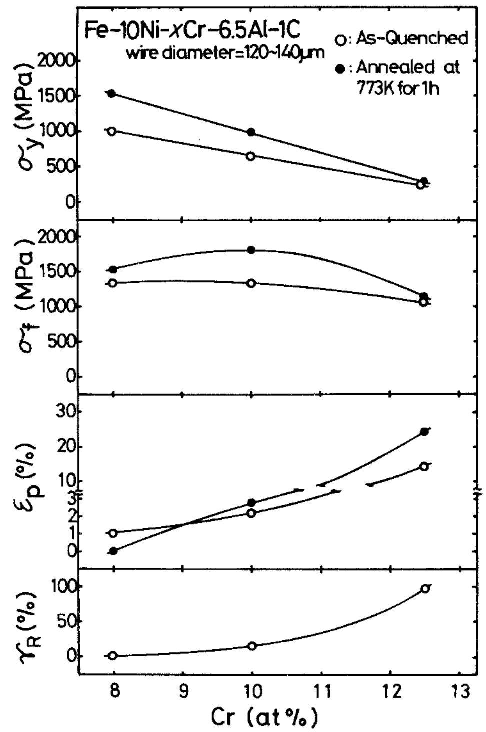

Figure 10 Changes in σ_y, σ_f, ϵ_p, and γ_R of melt-quenched Fe–10 Ni–Cr–6.5 Al–1.0 C wires with chromium content.

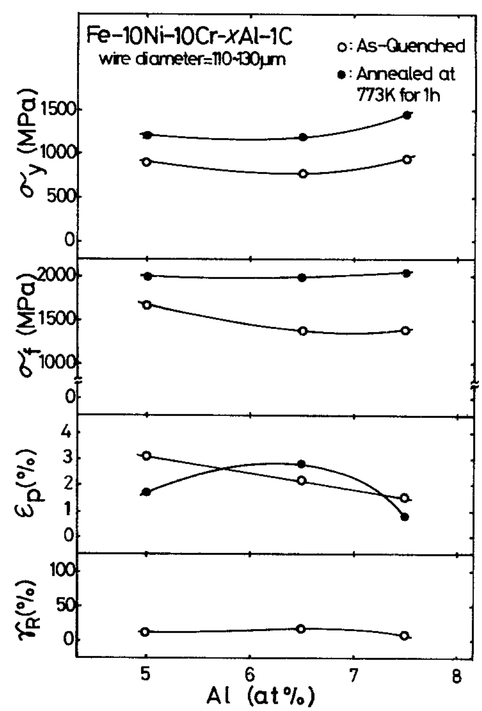

Figure 11 Changes in σ_y, σ_f, ϵ_p, and γ_R of melt-quenched Fe–10 Ni–10 Cr–Al–1.0 C wires with aluminium content.

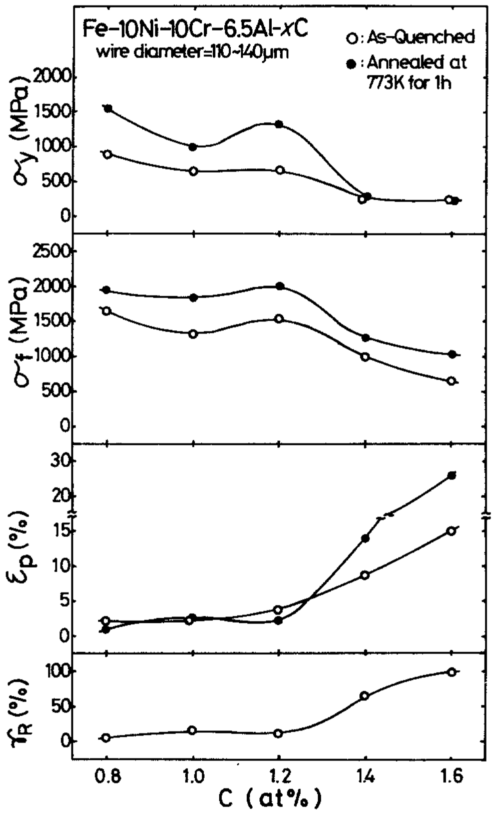

Figure 12 Changes in σ_y, σ_f, ϵ_p, and γ_R of melt-quenched Fe–10 Ni–10 Cr–6.5 Al–C wires with carbon content.

method [12, 13] is also presented for reference. In a series of Fe–Ni–10 Cr–6.5 Al–1 C alloys, σ_y and σ_f exhibit the highest values of 1080 and 1550 MPa in the as-quenched state and 1840 and 2060 MPa in the annealed state at 773 K for 1 h, respectively, for the 8% Ni wire having an almost completely lath martensite single phase and decreases monotonically with increasing γ_R (i.e. increasing nickel content). ϵ_p remains almost unchanged for the α'_L wires, increases significantly on the appearance of the γ-phase and reaches 17.5% for the γ single phase wire containing 12.5 at% Ni. Similar changes in σ_y, σ_f and ϵ_p as a function of γ_R amount were recognized for the other alloy series. Fig. 10 shows that the increase in chromium content from 8 to 12.5 at% causes the structural change from α'_L to γ_R, resulting in a gradual decrease in σ_y from 1000 to 250 MPa and σ_f from 1350 to 1050 MPa and an increase in ϵ_p from 1.0 to 14.5%. The increase in aluminium content from 5 to 7.5 at% in the series of Fe–10 Ni–10 Cr–Al–1 C alloys does not cause an appreciable change in the γ_R amount and hence there are no drastic changes in σ_y, σ_f, and ϵ_p with varying aluminium content, as seen in Fig. 11. Furthermore, the effect of carbon on σ_y, σ_f, ϵ_p, and γ_R in Fe–10 Ni–10 Cr–6.5 Al–C alloys is shown in Fig. 12. σ_y and σ_f of the annealed wires exhibit high values of 1550 and 1950 MPa in the α'_L single phase region containing less than about 1.3 at% C and decrease significantly with increasing carbon content (i.e. increasing γ_R content). On the other hand, ϵ_p exhibits a low value of $\simeq 2.5\%$ for the α'_L wires, but increases significantly with increasing γ_R and reaches about 15% for the γ_R wire containing 1.6 at% C. From Figs. 9 to 12, one can also notice a general tendency that the increases in σ_y and σ_f upon annealing at 773 K are greatest for the α'_L single phase and decrease with increasing γ_R content. One exception to the tendency is seen for the γ wire of Fe–10 Ni–10 Cr–6.5 Al–1.6 C alloy and the deviation is probably due to the remarkable increase in ϵ_p of the γ wire upon annealing.

3.5. Fracture morphology

Fig. 13 shows the tensile fracture surface morphology for the as-quenched and annealed (773 K, 1 h) α'_L wires of Fe–10 Ni–10 Cr–6.5 Al–1 C alloy. The generation of fine-scale ruggedness is densely seen over the fracture surface, suggesting that each unit in the fracture process which occurs by nucleation, growth and coalescence of microcavities is very fine and a relatively large amount of energy was spent during the fracture process. Furthermore, no appreciable distinct change in fracture morphology by annealing at 773 K is seen for the α'_L wire.

3.6. Comparison of microstructures, mechanical properties and thermal stability of α'_L with those of other metastable phases

In order to confirm the features of the structure, and mechanical properties of the α'_L wires in the Fe–Ni–Cr–Al–C system, the microstructure, σ_y, σ_f, ϵ_p average grain size, and thermal stability of the α'_L wires are summarized in Table I together with those of the other metastable phases in melt-quenched iron-based alloys reported previously. Also, the decompostion temperature of each metastable phase to equilibrium phases and their equilibrium phases are presented in the table for reference. The features of the table may be described as follows:

1. the metastable austenite (γ) and ordered

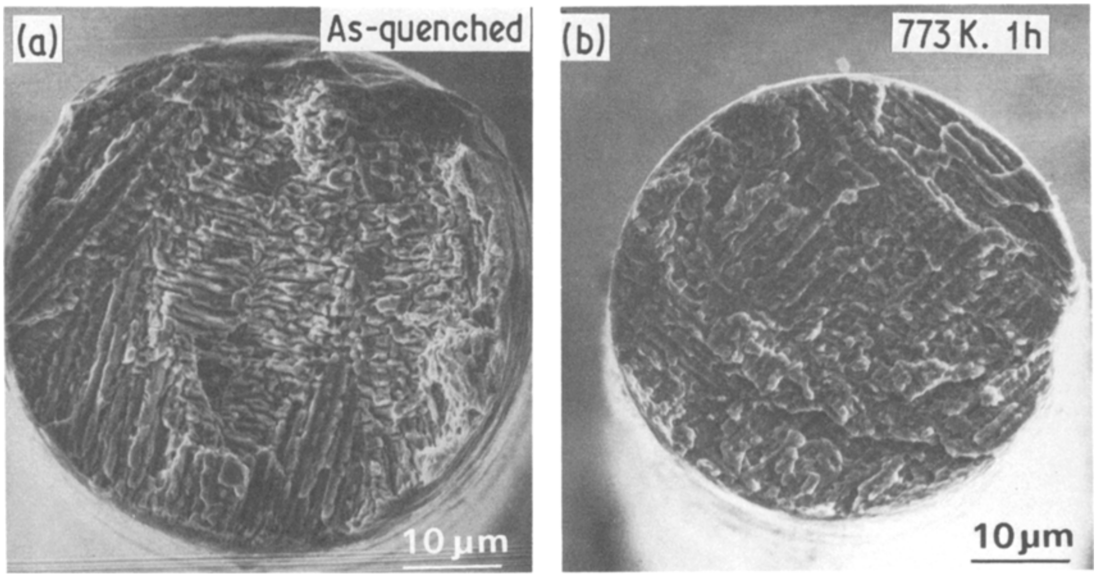

Figure 13 Scanning electron micrographs showing the tensile fracture morphology of melt-quenched Fe–10 Ni–10 Cr–6.5 Al–1.0 C wires. (a) as-quenched and (b) annealed at 773 K for 1 h.

austenite (γ') containing nickel or manganese possess a large elongation and low tensile strengths, even though one can see that the γ' phase of Fe–Ni–Cr–Al–C system exhibits high values of strengths as well as elongation;

2. the metastable austenite phase containing chromium, molybdenum or aluminium, being the ferrite-forming element, possesses relatively high strengths and a small elongation;

3. the bcc solid solution (α) and $L2_0$-type compound (β') exhibit low values of strengths as well as elongation and

4. the α'_L phase exhibits high values of σ_y and σ_f, and in particular the σ_f is the highest among a number of the metastable phases, even though ϵ_p is as small as about 1%.

It is thus to be noticed that the strengths of the low carbon α'_L steels prepared in the present work are comparable to those of the γ phase in the Fe–Cr–C system and the γ' phase in the Fe–Ni–Al–C system containing as much as about 6 to 8 at% carbon. This is interpreted as due to an inherent difference of strengthening mechanism between the α'_L phase and the γ or γ' phase; while the high strengths of the γ and γ' phases are due mainly to the solid solution strengthening of interstitial carbon element, those of the α'_L phase appear to originate from extremely high densities of dislocations and lath boundaries. Although the reduction of aluminium content in Fe–Ni–Cr–Al–C alloys is considered to cause the enhancement of ϵ_p of the α'_L phase without significant decreases in σ_y and σ_f, the reduction prevented the direct formation of the α'_L phase wires from liquid.

4. Conclusion

The wires of metastable α'_L phase exhibiting high strengths and relatively good ductility were produced in the Fe–Ni–Cr–Al–C system by the melt-quenching technique even though the usually solidified alloys are composed of a mixed structure of $\alpha + M_{23}C_6$. The wire production was carried out using an in-rotating-water spinning apparatus in which the melt was ejected through the orifice of a quartz nozzle into the rotating water layer. The α'_L wires thus obtained have a nearly circular cross section, and the wire diameter lies in the range 100 to 140 µm. The formation range of the α'_L wires is limited to the range of 7 to 11 at% Ni or Cr, 5 to 8 at% Al and 0.7 to 1.5 at% C and further increases in nickel, chromium and carbon result in a mixture of γ into the α'_L phase. The average lath size of the α'_L phase is about 0.3 µm in width and 2 µm in length. The σ_y, σ_f and ϵ_p of the α'_L wires are about 640 to 1080 MPa, 1300 to 1550 MPa and 1 to 3%, respectively, in the as-quenched state and annealing at 773 K for 1 h results in an increase of about 45 to 70% for σ_y and 30 to 45% for σ_f without distinct structural change. A further rise in annealing temperature causes a decrease in ϵ_p to about 0 to 1% through

TABLE I Microstructure, mechanical properties, and thermal stability of melt-quenched iron-based alloys having various metastable phases. Equilibrium phases and references are also presented

	Melt-quenched phase									
	α'_L	γ	γ	γ	γ	γ'	γ'	γ	α	β'
Alloy (at %)	Fe–8Ni–10Cr–6.5Al–1C	Fe–8Ni–10Cr–7.5Al–3C	Fe–17Cr–6.5C	Fe–6Mo–6.5C	Fe–8Al–8C	Fe–20Ni–16Al–6.5C	Fe–20Mn–16Al–6.5C	Fe–20Ni–7C	Fe–20Al–10Cr	Fe–25Al–5Mo
Sample shape	wire ($d \simeq 100\,\mu m$)	wire ($d \simeq 100\,\mu m$)	ribbon ($t \simeq 40\,\mu m$)	ribbon ($t \simeq 40\,\mu m$)	ribbon ($t \simeq 30\,\mu m$)	ribbon ($t \simeq 80\,\mu m$)	wire ($d \simeq 100\,\mu m$)	ribbon ($t \simeq 30\,\mu m$)	ribbon ($t \simeq 70\,\mu m$)	wire ($d \simeq 100\,\mu m$)
σ_y (MPa)	1100	470	1350	720	940	1200	650	750	560	450
σ_f (MPa)	1550	820	1400	800	995	1200	850	980	620	550
ϵ_p (%)	1	18	2	2	2	6	8	8	1	2
Grain size (μm)	width 0.3 length 2	3	0.2	0.2	0.2	3	10	0.4	10	2
Decomposition temperature (K)	723	823	773	673	773	773	773	773	923	923
Equilibrium phase	$\alpha + M_7C_3 + M_{23}C_6$	$\alpha + FeAl + M_7C_3$	$\alpha + Cr_7C_3$	$\alpha + Mo_2C$ (or Fe_2MoC)	$\alpha + Fe_3AlC + M_3C$	$\alpha + FeAl + M_3C$	$\alpha + FeAl + M_3C$	α + graphite	$\alpha + Cr_2Al$	Fe_3Al
Reference	present work	[7]	[15, 16]	[16, 17]	[18]	[19]	[6, 19]	[20]	[21]	[5, 22]

the phase decomposition of α'_L to $\alpha + M_7C_3 + M_{23}C_6$. The increases in the σ_y and σ_f on the low-temperature annealing appear to be due to the precipitation of an unidentified fine compound on the high densities of dislocations and lath boundaries. Thus, the present α'_L phase wire is very attractive as a high-strength material because of the direct production of the wire having a circular cross section from the liquid state.

References

1. A. INOUE, H. TOMIOKA and T. MASUMOTO, *J. Mater. Sci. Lett.* **1** (1982) 377.
2. *Idem, Met. Trans.* **14A** (1983) 1367.
3. *Idem, ibid.* **14A** (1983) 2319.
4. *Idem, J. Mater. Sci.* **19** (1984) 3786.
5. A. INOUE, T. MASUMOTO, H. TOMIOKA and N. YANO, *Inter. J. Rapid Solidification* **1** (1984) No. 2, in press.
6. A. INOUE, H. TOMIOKA, M. HAGIWARA and T. MASUMOTO, *Trans. Jpn. Inst. Metals* **23** (1982) 341.
7. A. INOUE, H. TOMIOKA and T. MASUMOTO, *Met. Trans.* **16A** (1985) No. 2, in press.
8. *Idem, Trans. Iron Steel Inst. Jpn.* **25** (1985) No. 9, in press.
9. A. INOUE, H. TOMIOKA, N. YANO and T. MASUMOTO, The Fifth International Conference on Rapidly Quenched Metals, Wurzburg, September (1984) to be submitted.
10. A. INOUE, H. TOMIOKA and T. MASUMOTO, private communication (1982).
11. I. OHNAKA, T. FUKUSAKO and T. DAIDO, *J. Jpn. Inst. Metals* **45** (1981) 751.
12. T. MASUMOTO, I. OHNAKA, A. INOUE and M. HAGIWARA, *Scripta Metall.* **15** (1981) 293.
13. B. L. AVERBACH and M. COHEN, *Trans. AIME* **176** (1948) 401.
14. R. L. MILLER, *Trans. Amer. Soc. Metals* **57** (1964) 892.
15. T. MINEMURA, A. INOUE, Y. KOJIMA and T. MASUMOTO, *Met. Trans.* **11A** (1980) 671.
16. T. MINEMURA, A. INOUE and T. MASUMOTO, *Trans. Iron Steel Inst. Jpn.* **21** (1981) 649.
17. T. MINEMURA, A. INOUE, Y. KOJIMA and T. MASUMOTO, *ibid.* **22** (1982) 934.
18. A. INOUE, T. MINEMURA, A. KITAMURA and T. MASUMOTO, *Met. Trans.* **12A** (1981) 1041.
19. A. INOUE, Y. KOJIMA, T. MINEMURA and T. MASUMOTO, *ibid.* **12A** (1981) 1245.
20. *Idem, Trans. Iron Steel Inst. Jpn.* **21** (1981) 656.
21. T. NAOHARA, A. INOUE, T. MINEMURA, T. MASUMOTO and K. KUMADA, *Met. Trans.* **13A** (1982) 337.
22. A. INOUE, N. YANO and T. MASUMOTO, unpublished research (1984).

Received 17 August
and accepted 13 September 1984